Structural Reorganization on Amorphous Ice Films below 120 K Revealed by Near-Thermal (~1 eV) Ion Scattering

Jobin Cyriac and T. Pradeep*

DST Unit on Nanoscience (DST UNS), Department of Chemistry and Sophisticated Analytical Instrument Facility, Indian Institute of Technology Madras, Chennai 600 036, India

Received: December 11, 2007; In Final Form: January 18, 2008

Topmost layers of amorphous ice undergo a structural transformation before the onset of crystallization and well before the premelting transitions. Ultralow-energy (~1 eV) mass-selected Ar^+ scattering has been used to detect this structural change. The transformation is manifested in the form of drastic changes in the scattered ion intensity in the ≤2 eV collision energy range. The changes are limited to the first few monolayers as larger thicknesses produce no additional effects. The technique becomes chemically sensitive but insensitive to the morphology and structure as the energy is increased above 3 eV. A similar behavior is observed with He^+, Kr^+, and a polyatomic ion, CH_3^+. Experiments revealed that the structural changes occurred only on amorphous ice and no such change occurred on crystalline ice. H_2O and D_2O ices behave similarly.

Introduction

Ice, the condensed phase of water, not only exists on the surface of Earth but also throughout our planetary system and interstellar space. The structural transformations and reactivity of water ice have fascinated chemists and astrophysicists for long. Despite its simplicity in the molecular level, the phase diagram of water ice is complex. Recently, it was reported that a metastable proton-ordered form of ice XIV can be formed under kinetically controlled conditions.[1] Ice can exist in 15 different crystalline phases, apart from its low density and high density amorphous forms.[1,2] The structure of the ice surface in molecular detail is an interesting area of research since it can be considered as a model system for several investigations. The reactivity of the ice surface is understandably sensitive to its structure. There is still controversy about the fundamental properties of ice including crystallization and glass transition temperatures.[3] The conventional estimate and widely accepted glass transition temperature, however, is 136 K.[4] There are others who suggested that this value should be reassigned as ~160 K.[5,6] Phenomena such as the existence of viscous liquid layers,[7] supercooled water,[8] surface premelting,[9] and so on are still under debate. The viscous layer persisting on the ice surface in the temperature range 140−210 K has been called the "restrained amorphous form".[10] Due to this strain, the morphology of ultrathin ice film changes when it is warmed above 140 K. A metastable supercooled extension of normal liquid water exists when amorphous solid water (ASW) crystallizes near 160 K.[8] Surface premelting transitions start at a higher temperature. It is commonly believed that the surface premelting or the formation of quasi-liquid layer on the surface starts around 243 K.[9] An intriguing study shows the nonlinear dynamics of adsorbate molecules over melting ice.[11] Other interesting phenomena observed around the temperature range 100−150 K are micropore collapse[12] and ferrolelctricity in ice due to proton reorientation, both of which occur in the ice bulk.[13] Ferroelectricity refers to the existence of a net polar ordering

of water molecules in the ice films prepared on a metal substrate. While proton ordered ice is expected to be thermodynamically stable only below 100 K,[14] such an order has been reported in the first ~20 monolayers (ML) (close to the substrate) grown on Pt(111) in the temperature range of 120−137 K.[13] A recent study by McClure et al. suggested that ice is nonfragile below a temperature of 160 K.[6] From these reports it is clear that the transformation/reorganization within and on top of ice is fascinating but a controversial area of science. Understanding of any structural changes on ice surface is important since transport properties and adsorption/desorption behaviors are strongly related to such phenomena. In this paper, we present the use of *ultralow*-energy mass-selected Ar^+ (He^+, Kr^+, and CH_3^+) scattering experiments to probe the *structural changes on the very top of the ice surface*.

Vibrational spectroscopy,[15] electron diffraction,[10] X-ray absorption spectroscopy,[16] electron spectroscopy,[17] TPD,[18] Kelvin probe,[13] and secondary ion mass spectrometry (SIMS)[19] are some of the experimental techniques used to understand the physics and chemistry of ice. Several of these techniques have been employed to investigate surface structure and morphological changes of amorphous ice. Another method called low-energy ion scattering (LES) successfully demonstrated its sensitivity toward ice surface and the reactions occurring on it.[20] Using Cs^+ reactive ion scattering spectroscopy (RIS), a LES method, one can study the topmost layers of the ice surface.[21] Although low-energy (≤100 eV) atomic and polyatomic ion scattering are sensitive to the chemical nature of the surface,[22] here we show that Ar^+ and other ions of ~1 eV collision energy are extremely sensitive to the surface morphology and/or structure. These experiments show that molecularly thin layers of amorphous ice undergo a structural transformation below the onset of crystallization[10] and well before the existence of liquid layers observed above 140 K.[7] The technique becomes chemically sensitive but insensitive to the morphology and/or structure as the collision energy is increased to 3−4 eV. This transformation is confirmed with other projectiles such as He^+, Kr^+, and CH_3^+ in the same collision energy window. It is well-known that crystalline and amorphous ice show significant difference

* To whom correspondence should be addressed. E-mail: pradeep@iitm.ac.in. Fax: 91-44-2257 0545/0509.

in surface chemical behavior due to the difference in their hydrogen bonding ability.[23,24] Microscopic changes occurring on the top layers of amorphous ice can lead to significant differences in their interactions. From the earlier discussions, it is clear that a variety of surface dynamics occur on the ice surface before melting in the bulk. The transformation revealed here might be important in determining the reactivity of molecules and ions impinging on ice particles at low temperatures.

Experimental Section

The experiments described here were carried out in a double-chamber UHV apparatus (base pressure $<5.0 \times 10^{-10}$ mbar) equipped with ion scattering facilities described elsewhere[25,26] (see also Supporting Information Figure S1). Briefly, mass- and energy-selected ions were directed onto the surface of choice and the scattered ions were mass analyzed. For the experiments described here, Ar^+ (or He^+, Kr^+, and CH_3^+) were generated from ultrahigh-purity Ar (or He^+, Kr^+, and CH_3^+) gas by electron impact at 70 eV and subsequently mass selected by a quadrupole mass filter. Ar (or He, Kr, and CH_4) gas was introduced into the ionization chamber through a leak valve during which the pressure in it was raised to 1.0×10^{-7} mbar. The ions were transferred into a quadrupole mass filter (Q1) through a set of einzel lenses. It was possible to get the projectile ions of different collision energy in the range 1−100 eV by varying the potential of the ion source block and tuning the rest of the ion optics to get a beam current of 1−2 nA. Note that no potential was applied on the surface in a typical scattering experiment. The ions collide with the surface at an angle of 45° with reference to the surface normal, and the scattered ions were mass analyzed by a quadrupole mass analyzer (Q3). A high-precision UHV sample translator with *xyz* axis movement and tilt facility was used as the substrate holder. A 10 × 10 mm polycrystalline copper sheet was used as the substrate for deposition in these experiments. Two K type thermocouples simultaneously measured the temperature. Sample cooling was achieved by liquid-nitrogen (LN_2) circulation, and the minimum temperature attained was 110 K, which could be reached within 20 min. The temperature resolution of the controller was 1 K.

We measured the energy spread of primary ion beam by varying the potential at the surface. The spectrometer was tuned for the desired energy collision (keeping the surface at ground potential). Q1 was tuned for Ar^+, and Q3 was set to detect the scattered ions. At this point, the scattered ion intensity was measured as an average of 10 spectra, each of which was an average of 100 scans. The potential at the surface was varied in steps of 200 mV. The intensities of the scattered ions were plotted to determine the energy width. The variation in primary ion intensity as a function of surface potential at 1 eV Ar^+ collision is given in Figure 1. The measured full width at half-maximum (FWHM) of the 1 eV Ar^+ beam was ∼62%. The energy spreads of 3 eV (inset of Figure 1) and 5 eV were ∼11.5%. Typically the energy spread is around this value until about 10 eV. However, at 1 eV, much larger width is obtained. It appears that at this energy the ion optics could not be optimized perfectly. Data corresponding to other collision energies are given in Supporting Information Figure S2. No other ions contribute to the scattered ion intensity in this energy window. Distortion from a Gaussian distribution of incident ion kinetic energy[27] is due to the nonideal transmission characteristics of the lenses.

Deionized water, after triple distillation, was used for preparing solid water. D_2O and $C_2H_2Cl_4$ were purchased from Aldrich
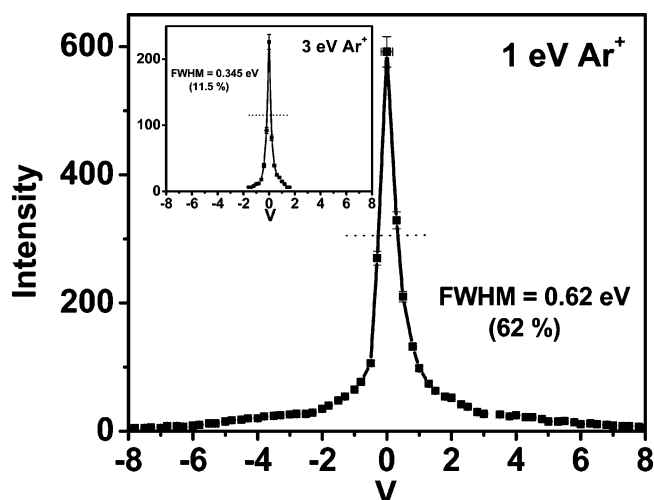

Figure 1. Plots of ion intensity as a function of retarding/accelerating potential at 1 and 3 eV (inset) collision energies. Experiments were done at room temperature after floating the Cu substrate. The collision energies mentioned correspond to a potential of 0 V on the target plate. A 4% fluctuation in the intensity is indicated. The voltage applied had 20 mV fluctuation at the value mentioned.

chemicals. These liquids were purified by several freeze−pump−thaw cycles on each day of the experiment. Thin layers of molecular solids were grown from vapor phase on a polycrystalline copper surface maintained at specific temperatures. The deposition flux of the vapors was adjusted to ∼0.1 Langmuir (L)/s. The thickness of the overlayers was estimated taking 1.33×10^{-6} mbar/s = 1 L. This is roughly equivalent to 1 ML (monolayer) since the sticking coefficient is nearly unity. The coverage was not determined exactly by other techniques. The ice film grown this way in ultrahigh vacuum is known to be amorphous in nature (ASW). The 50 ML ASW was grown by depositing water vapor at 1×10^{-7} mbar on a precooled copper substrate kept at 110 K. A tube doser of 3 mm diameter kept 12 mm away from the target plate avoided significant deposition on other cold parts of the instrument. To prepare crystalline water (CW), 50 ML of ASW (prepared at 110 K) was heated to 145 K and kept at that temperature for 5 min. The desorption rate of ice at this temperature is negligible. Crystallization induced dewetting,[28] and consequent exposure of the underlying copper surface is very unlikely at this large thickness. It has been noted that the dewetting temperature is much higher (∼160 K) for 50 ML ice films.[29] The surface prepared was analyzed with 30 eV Ar^+ to confirm the presence of ice on the substrate. The surface was further cooled to 110 K to perform the temperature-dependent scattering experiments or further deposition. Deposition was also done at various temperatures. Every spectrum was averaged for 50 scans, and 10 such averaged spectra were further averaged to get a statistically reliable intensity reading in the plots presented. The estimated error in the intensity was about 4% and shown as error bar in Figures 2, 3, and 5. The formation of ASW and CW films was confirmed by infrared spectroscopy of ice films grown on KBr disks in a separate chamber.

Results and Discussion

The variations in scattered ion intensities from 50 ML ASW, 50 ML CW, and clean Cu are plotted against temperature in Figure 2. The scattered Ar^+ intensity from ASW shows drastic increase below 120 K, before the onset of crystallization (Figure 2). In absolute terms, the intensity doubles between 110 and 125 K. Such a change was absent in the case of CW. A similar
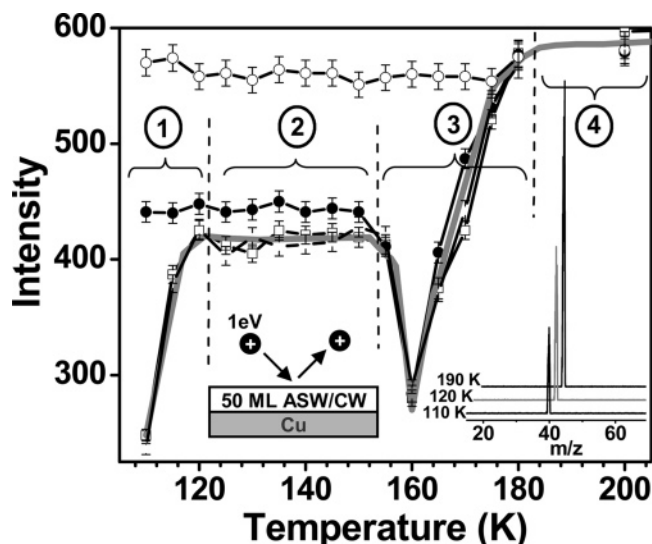
Structural Reorganization on Amorphous Ice Films

J. Phys. Chem. C, Vol. 112, No. 13, 2008 **5131**

Figure 2. Scattering intensity variation of 1 eV Ar^+ collisions at bare copper ($\bigcirc$), 50 ML ASW(H_2O) ($\square$), 50 ML ASW(D_2O) ($\blacksquare$), and 50 ML CW(H_2O) ($\bullet$). The continuous gray line shows an approximate representation of the overall behavior of ASW. Inset: Typical Ar^+ scattering mass spectra of 50 ML ASW for three different temperatures and averaged for 50 scans. The collision energy was 1 eV. Note the drastic change in the intensities as a function of temperature. A schematic of the process is shown.

Figure 3. Intensity of 1 eV Ar^+ as a function of temperature for (a) 3 ML ASW ($\triangle$), (b) 6 ML ASW ($\blacktriangle$), (c) 1 ML ASW ($\blacktriangledown$), and (d) 50 ML CW@3ML ASW ($\triangledown$). The curve obtained for (e) 50 ML CW ($\bullet$) is shown for comparison. It is clear that the transition seen in region 1 is due to the ultrathin ice layers. A schematic of the process for (d) is shown.

change was observed in D_2O ice (D_2O-ASW) prepared similarly. However, the intensity from pure Cu substrate remains the same throughout. Thus, the observed raise in intensity in ASW suggests a drastic change for this surface, distinctly different from others. The reproducibility of each of these curves at every point of the data presented was investigated. The intensity of Ar^+ from 50 ML ASW maintained at 110 K was retained even after 1 eV Ar^+ collision for 1 h. The low ion flux used was inadequate to induce any structural changes on the ice surface. Moreover, the variation in intensity was completely reproducible in experiments extended over several months. Typical scattering spectra at a few temperatures are shown in the inset of Figure 2. The quality of the data is evident from the spectra presented.

Overall behavior of the scattered ion intensity (gray trace) shows four distinct regions (separated by dashed lines) in the figure. It can be seen immediately that region 4 is due to pure copper as it is the same in all cases investigated, and it occurs at a temperature after complete desorption of water. Region 3 coincides with the desorption temperature of water, and the decrease in Ar^+ intensity is likely to be due to large neutralization while water is desorbed from the surface (we will come back to this aspect later). The ion neutralization can occur anywhere during the ion flight. In region 2, i.e., above 120 K, a small decrease in ion intensity is observed which may be attributed to the changes in the molecular orientation on the top ice layers. This leaves region 1, which is attributed to a structural transition in ASW. No other change, except a structural one, can occur at this temperature as no desorption occurs. As the ions are sensitive only to the very top molecular layers at this energy, we suggest that this transition corresponds to the outermost layers. This aspect is discussed later in the paper. This transition is different from that reported by Zondlo et al.,[12] which is derived from the surface of micropores within the ice bulk. Other than this micropore collapse, the available literature on the changes occurring at this temperature window involves the proton reorganization or the so-called ferroelectric state of ice. Su et al.[30] showed that ice is ferroelectric in the temperature range 120−137 K. Ferroelectric polarization ob-
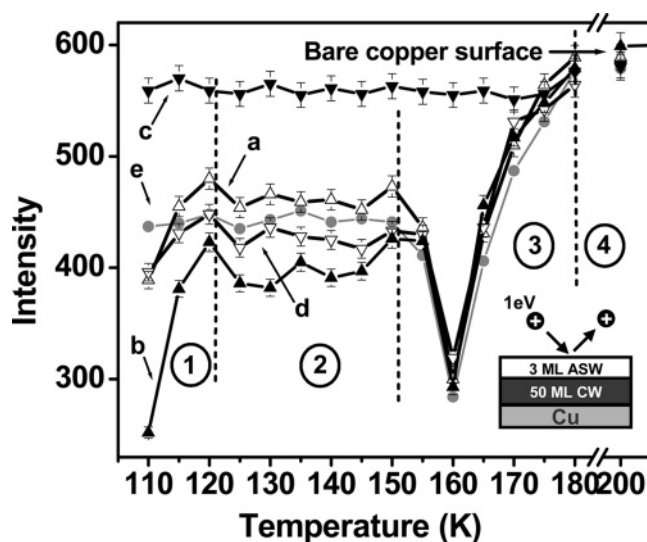
served by Iedema et al.[13] disappears largely between 50 and 80 K, with traces continuing up to 150 K. The ordering shows a weak maximum between 120 and 150 K for 2200 ML ice deposited at 110 K. The present changes probed by ultralow-energy Ar^+ scattering did not show any transition other than the change at ~120 K. The deposition temperature has not affected the scattered ion intensity; the structural transformation is present for all samples deposited below 115 K, and for those deposited above this temperature, it is absent (Supporting Information Figure S3). The scattering intensity is matching exactly for all ices deposited up to a temperature of 135 K. As noted before, CW, which formed at 145 K and cooled to 110 K, shows a different scattered ion intensity. Therefore, the above-mentioned transformation is purely due to the structural reorganization on the top layers of thin ice films. We have also checked the reversibility of the process by preparing 50 ML ice films at various temperatures and cooling them to 110 K (Supporting Information Figure S4A). As expected, the transition was not observed in these samples. Experiments were repeated with 50 ML ice films deposited at 110 K and annealed at different temperatures and further cooled to 110 K to start the scattering experiments (Supporting Information Figure S4B). The irreversibility of the transformation was confirmed by these experiments. From Figure 2 we see that there is a small difference in the intensity of scattered ions from ASW and CW even after the bulk crystallization of ASW. This implies that there are distinct changes in the surface structure of ASW throughout the 125−150 K window. Besides the low-temperature transition, there are also other reproducible small variations in the scattered ion intensity in this temperature window, signifying subtle changes on the surface.

Effect of Thickness. The coverage dependence of the scattering intensity from ASW and CW surfaces was investigated in the energy range 1−20 eV. For 1 eV Ar^+ scattering, 3 ML coverage of ASW (Figure 3, trace a) gave values different from 50 ML ASW. But when the thickness of the film was increased to 6 ML (trace b), the intensities of the scattered ions were the same as that of 50 ML ASW (compare with Figure 2). This implies that the variation in the intensities of Ar^+ is mainly due to structural changes occurring on the *surface* layers.

The intensity variation is absent for 1 ML ASW film (Figure 3, trace c). At lower (1 ML and submonolayer) coverages, the possibility of island formation exists.[28] Experiments at various coverages suggest that the observed change occurs only on the very top layers of the surface. To get further insight into this difference in scattering intensity, different systems have been investigated in a similar way. An experiment with 50 ML CW@50 ML ASW (ASW over CW) gave the same curve as 50 ML ASW in Figure 2 (data not shown). Thus, the *surface* morphology of the 50 ML ASW film was not affected by the underlying CW layer although the CW substrate is known to induce crystallization of ice overlayers at 128 K (instead of 136 K in parent ASW).[31] But a lower coverage of ASW on CW (50 ML CW@3 ML ASW) resulted in dissimilar ion intensities compared to 50 ML CW@50 ML ASW. For 3 ML ASW and 50 ML CW@3 ML ASW (Figure 3, traces a and d), the scattered ion intensity is the same at 110 K. But the intensity is different in the 120−150 K range. This difference may be due to the subtle differences in surface morphologies of the systems investigated. Also, we have conducted the experiments at higher coverages of ASW to illustrate the effect of larger thickness. Higher coverages like 100, 150, and 200 ML produced the *same* intensities as in the case of 50 ML ASW. Therefore, the increase in thickness did not have any effect on the scattered ion intensities. It is a further confirmation for the argument that the observed phenomenon is entirely due to the *surface layers* and not due to any proton ordering[13] which shows a coverage dependence. Another important conclusion from this set of experiments is the wetting nature of the Cu substrate. It is clear that a coverage of >6 ML ASW always produced the same ion intensities. Therefore, Cu substrate is not exposed to the projectile ions or Ar^{+} collision did not sputter off the ASW layers from the substrate. It is reported that ∼5 eV Xe atom sputtering is able to lift off 1 ML ASW from Pt(111) substrate[29] implying dewetting. Thus, it can be concluded that ice layers of thickness <6 ML may not cover the surface completely while above this coverage; the ice film is continuous on a polycrystalline Cu substrate.

Effect of the Substrate. We have studied substrate effects by preparing a 50 ML film of $C_2H_2Cl_4$ first on copper substrate and making ASW films over it (see Figure 4). This molecule was selected because the desorption temperature of solid C_2H_2-Cl_4 is ∼185 K, higher than the water desorption temperature in the present experimental conditions. It was found that in these $C_2H_2Cl_4$@ASW systems, above 6 ML ASW, the intensities are similar to those of the ASW films prepared on bare copper substrate. Intensity variation as a function of temperature for 50 ML $C_2H_2Cl_4$@50 ML ASW and 50 ML $C_2H_2Cl_4$@10 ML ASW is given in Figure 4a,b. These curves are very much identical with the curves given in Figures 2 and 3. It is known that $C_2H_2Cl_4$ molecules cannot penetrate through ice overlayers.[25] So the intrusion of $C_2H_2Cl_4$ molecules in the neutralization process in this study can be ruled out. The thickness of C_2H_2-Cl_4 was varied from 10 ML to higher coverages, and it was found that the intensities were remaining the same. Similar experiments were done with the CW film, i.e., $C_2H_2Cl_4$@CW systems, which did not lead to a different conclusion (Figure 4c). These experiments confirmed that the transformation at 120 K is independent of the substrate. The sudden drop in ion intensity at ∼160 K was found in these cases also, which indicates that the desorption of molecules was the principal cause of the increased neutralization of Ar^{+} at this temperature regime. It may be suggested that the dangling −OH remaining on the surface after multilayer desorption can lead to ion intensity
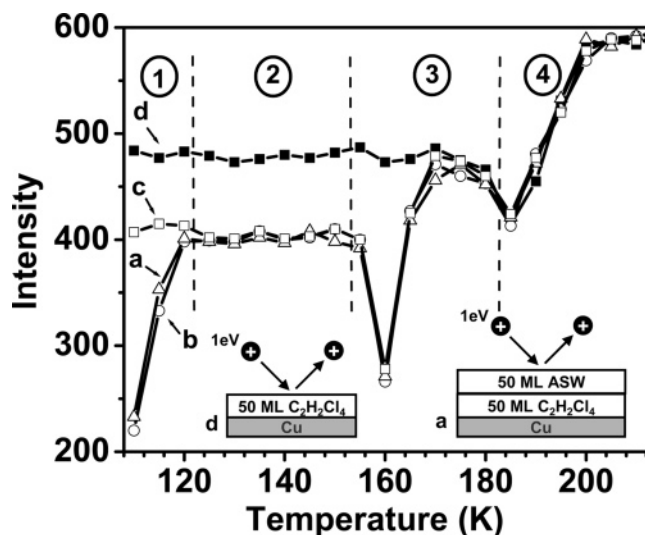

Figure 4. Intensity variation of 1 eV Ar^{+} as a function of temperature for different ice films prepared on predeposited $C_2H_2Cl_4$ substrate: (a) 50 ML $C_2H_2Cl_4$@50 ML ASW, (b) 50 ML $C_2H_2Cl_4$@10 ML ASW, and (c) 50 ML $C_2H_2Cl_4$@50 ML CW. A blank experiment done with 50 ML $C_2H_2Cl_4$ is given as (d). Schematics for (a) and (d) are shown. The error bars have been omitted for clarity.

decrease. But the dip in intensity at ∼160 K with a different substrate ruled out this possibility. In addition, the extent of intensity reduction at ∼160 K is the same as that for a pure ASW surface suggesting that there is no effect due to residual dangling −OH (in Figure 2), after multilayers of water are desorbed. The intensity dip at ∼185 K, wherever $C_2H_2Cl_4$ was used as substrate, is another supporting piece of evidence of the increased neutralization of ultralow-energy Ar^{+} ions via the desorption of the surface species. There was no drop in Ar^{+} intensity around 160 K in the blank experiment conducted with 50 ML $C_2H_2Cl_4$ alone (Figure 4d). Since we are interested in structural rearrangement in ice films, the desorption induced neutralization was not investigated in detail. The data presented above further support our suggestion that the observed transition at ∼120 K is not due to ferroelectric polarization as it commences from the substrate−overlayer interface[30] and therefore should be affected by the presence of $C_2H_2Cl_4$. Experiments conducted with CH_3OH surfaces further confirmed the increased neutralization via desorption (Supporting Information Figure S5). A large decrease in scattered ion intensity was observed in the 130−155 K window due to the desorption of CH_3OH molecules. The desorption of methanol was visible as pressure increase in the vacuum gauge, starting at ∼130 K. Because of this, crystallization of methanol, supposed to occur at 120 K,[32] was indistinguishable. Moreover, we doubt whether the crystallization in methanol could be observable as a change in ion intensity since the crystallization of water ice was not reflected in ion intensities. The data for the CH_3OH−ice system is complicated due to the desorption process as well as intermixing. Therefore, other aspects of this system were not pursued further.

Higher Collision Energies. An increase in collision energy leads to decrease in scattering intensity. This is because of the increased neutralization events (Figure 5). The change as seen in region 1 is clearly visible with 2 eV Ar^{+} collision, and there is substantial intensity difference with the CW surface (inset of Figure 5). The variation in intensity with temperature is visible even at 3 eV and above whereas the scattered ion intensity is insensitive to the surface reorganization and ice desorption (see the trace for 8 eV, Figure 5). The high penetrating power of Ar^{+} ions at higher collision energies leads to more effective

Structural Reorganization on Amorphous Ice Films

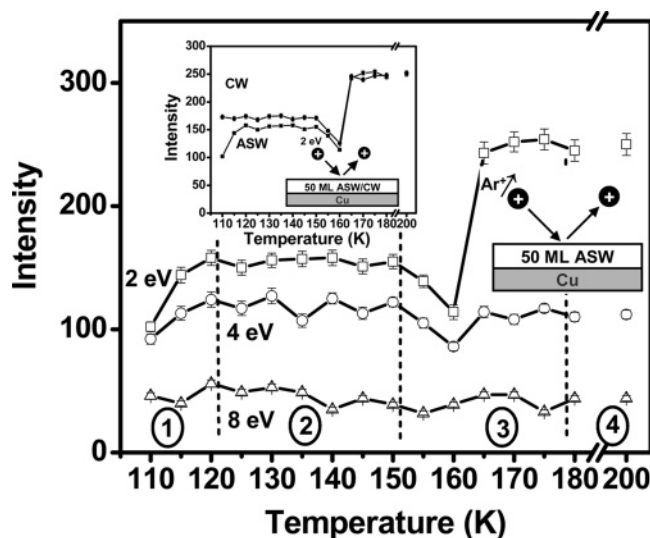*J. Phys. Chem. C, Vol. 112, No. 13, 2008* **5133**

Figure 5. Intensity variation as a function of temperature for 50 ML ASW at different collision energies: 2 eV (□); 4 eV (○); 8 eV (△). Four regions are separated with dotted lines. Inset: Comparison of the scattering intensity for 2 eV Ar^+ collisions on 50 ML ASW (■) and 50 ML CW (●). The distinction between ASW and CW surfaces is clearly visible with 2 eV collisions also. A schematic of the collision event is shown; the arrow near Ar^+ implies that the experiment involves variation of the collision energy.
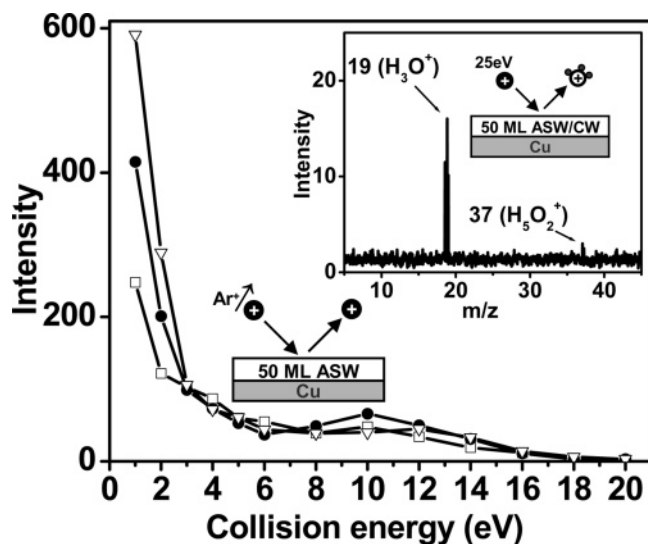

Figure 6. Scattered Ar^+ intensity as a function of collision energy for different surfaces: clean Cu (▽); 50 ML CW (●); 50 ML ASW (□). A schematic of the collision event is shown; the arrow implies that the experiment involves variation of the collision energy. Inset: Chemical sputtering spectrum from 50 ML ASW at 110 K. The collision energy of Ar^+ was 25 eV. A schematic of the sputtering event is shown.

trapping and subsequent neutralization. So the minor changes in the surface structure are unable to be captured by the primary ions.

When the collision energy is above 15 eV, the scattered ions do not contain Ar^+ (Figure 6). The curves obtained after a collision energy of 8 eV and above give the same intensity pattern irrespective of the surface. Low-energy sputtering from the surface starts only above 20 eV collisions and is observable in the resultant mass spectra (inset of Figure 6).[25,26] Chemical sputtering of ice surface yields H_3O^+ as reported earlier.[25] As the structural changes are better observed by low-energy ions and are seen only below 120 K, we conclude that this rearrangement is not ion-induced.
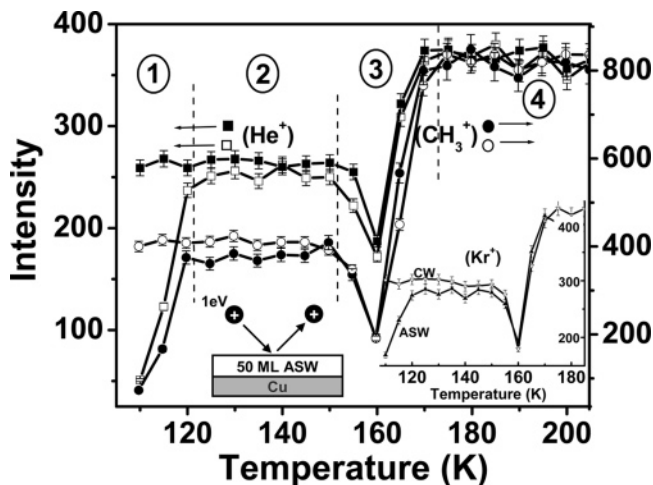

Figure 7. Scattering intensity variation of 1 eV He^+ and CH_3^+ collisions at ice surfaces: 1 eV He^+ at 50 ML ASW (□) and 50 ML CW (■); 1 eV at CH_3^+ at 50 ML ASW (●) and 50 ML CW (○). Inset: Kr^+ scattering intensity variation from 50 ML ice surfaces. A schematic of the process is also shown.

Effect of Deposition Temperature. To check the effect of ice deposition temperature on this structural reorganization, ice films were prepared at different temperatures and analyzed by 1 eV Ar^+. The intensities observed from these surfaces coincide with those from the ASW surface prepared at 110 K when compared at corresponding temperatures (Supporting Information Figure S3). Ice samples prepared above 120 K do not show the transition. This experiment ruled out the possibility of reorganization due to temperature ramping (from lower to higher) as an explanation for the observed change. Again, this is a confirmation of the absence of ion-induced structural changes on the surface. It could be argued that the observed intensity changes coincide with the contact potential difference seen for ice deposited at 110 K.[13] However, changes in contact potentials occur over a larger window of temperature in contrast to the drastic changes in intensity in a narrow temperature window observed here. Also such changes in proton ordering happen very close to the substrate and not at the surface−vacuum interface.

Various Projectile Ions. We have extended this study to other projectile ions such as He^+, Kr^+, and a polyatomic ion, CH_3^+, to understand the phenomenon in detail. Figure 7 shows the scattered ion intensity as a function of temperature for these ions. It is interesting to note that all of the ions are showing drastic increase in intensity at ~120 K for the 50 ML ASW surface. These experiments imply that the observed reorganization is not specific to the nature of the projectile ion, provided only low-energy scattering events take place. Region 3 of all the three noble gas ions (see Figures 2 and 7) is showing more or less the same minimum at 160 K, which indicates that this region is entirely interrupted by the desorption of water from the substrate. The polyatomic ion, CH_3^+, also reflects the changes occurred on the ASW surface through its intensity variation. Comparative discussion on the scattering behavior of various ions is given below.

Interpretation. At extremely low energy, ion interactions with surface are not only due to the translation energy but their potential energy also plays an important role. Trapping and neutralization are important events in the 1−3 eV energy range which decide the scattered ion intensity. There are two major factors important to consider. First, below 120 K, micropores are abundant on the top layers of ASW.[33] Reorganization occurring on the surface above 120 K may lead to the collapse

of the micropores, thereby reducing the trapping efficiency. Second, the work function of the surface has a major role in ion intensity. For a work function of the order 2 eV, resonant neutralization (RN) is thought to be the dominant mechanism for noble gas ions.[34] As a result of the large number of dangling $-OH$ and surface roughness, the work function of ASW (2.45 eV) is lower than that of CW (2.75 eV).[35] In comparison, copper has a much higher work function (4.6 eV).[36] From this, it may be suggested that the rearrangement occurring at 120 K leads to a reduction in the dangling $-OH$ and thereby increasing the work function, reducing neutralization. But another process, namely neutralization by trapping, also plays an important role. The thermodynamic advantage of neutralization is more for CW than for ASW surface, and this difference is the same for all the ions. The ionization potentials of He^+, Ar^+, Kr^+, and CH_3^+ are 24.5, 15.8, 14.0, and 15.5 eV, respectively. Normalized intensities of these ions would give an easy understanding of difference in neutralization without the effect due to the variation in the input flux. Such a comparison is given in Supporting Information Figure S6. The intensity difference between the data above and below 120 K in each case is likely to be the same if resonant neutralization was the sole mechanism responsible for the experimental observation. This being not the case suggests that neutralization via trapping in the surface layers plays a major role in bringing about the observed intensity variations. The trapping efficiency and subsequent neutralization of ASW surface toward the four ions (including Ar^+) are different. The relative variation in ion intensity between 110 and 125 K is given in Supporting Information Figure S6B by normalizing various ion intensities by the intensity at 110 K. It is clear that neutralization events occurring with Ar^+ and Kr^+ (comparable sizes) are similar and these are reflected in their intensities at various temperatures (see Supporting Information Figure S6B). The lower mass ions, He^+ and CH_3^+, are more effectively trapped than others. This is clearly seen in the spectrum when the scattered ion intensity before and after reorganization is compared. The size of He^+ and affinity (also size) of CH_3^+ to ice are the reasons for effective trapping and their similar scattered ion yield at 110 K. Lower size ions can be accommodated better in the surface pores making them lose their momentum. The interaction of the hydrogens of CH_3^+ with those of ice surface leads to greater retention time scales and hence increased neutralization efficiency. Reduced trapping and a decrease in affinity due to reduction in dangling $-OH$ increases the ion yield after the reorganization. However, there is a distinct difference between the He^+ and CH_3^+ data above 120 K. Above 120 K, the chemical interaction between CH_3^+ and ice can be attributed to the reduced scattered ion yield, in comparison to He^+. Above the reorganization temperature, the fraction of scattered ion intensity is almost the same for all the noble gas ions investigated. So it is clear that trapping at the surface layers is the principal neutralization mechanism at 110 K. Thus, the structural change at the top layers is suggested to be due to micropore collapse which leads to reduction in population of dangling $-OH$ bonds.

In conclusion, we show that a new structural transition occurs below 120 K on the surface layers of ASW, which can be picked up by near-thermal energy Ar^+ (and He^+, Kr^+, and CH_3^+) scattering. Upon closer examination of the scattered ion intensity, we observe a few other distinct changes, although these are not completely clear at this point. Effect of substrate was checked, and it was found that ASW deposited even on organic molecules manifested the same structural change indicating that the observed phenomenon is not substrate-induced. A drop down

in intensity was observed when the desorption of water takes place from the surface, and this large desorption induced neutralization was confirmed with experiments using $C_2H_2Cl_4$ and CH_3OH. The specificity of the transition to the surface is established by control experiments. Analogous data were observed using He^+, Kr^+, and CH_3^+ projectiles. The subtle structural changes lead to changes in the porosity and electronic structure and hence variation in the neutralization process. This reorganization may have implications to the chemistry of ice, and it suggests that one has to be aware of the changes in surface structure while investigating reactivity of ice surfaces at these temperatures.

Supporting Information Available: Experimental procedure, energy spread of 5 and 10 eV Ar^+, intensity variation as a function of temperature for 50 ML ASW prepared by depositing water vapor at various temperatures, data for samples deposited or annealed at various temperatures, intensity variation as a function of temperature for 50 ML MeOH, and normalized ion intensity versus temperature for all the projectiles for 1 eV collision. This material is available free of charge via the Internet at http:/pubs.acs.org.

References and Notes

(1) Tribello, G. A.; Slater, B.; Salzmann, C. G. *J. Am. Chem. Soc.* **2006**, *128*, 12594.

(2) Lobban, C.; Finney, J. L.; Kuhs, W. F. *Nature* **1998**, *391*, 268.

(3) (a) Yue, Y. Z.; Angell, C. A. *Nature* **2004**, *427*, 717. (b) Angell, C. A. *Chem. Rev.* **2002**, *102*, 2627.

(4) Johari, G. P.; Hallbrucker, A.; Mayer, E. *Nature* **1987**, *330*, 552.

(5) Minoguchi, A.; Richert, R.; Angell, C. A. *J. Phys. Chem. B* **2004**, *108*, 19825.

(6) McClure, S. M.; Safarik, D. J.; Truskett, T. M.; Mullins, C. B. *J. Phys. Chem. B* **2006**, *110*, 11033.

(7) Jenniskens, P.; Banham, S. F.; Blake, D. F.; McCoustra, M. R. S. *J. Chem. Phys.* **1997**, *107*, 1232.

(8) Smith, R. S.; Kay, B. D. *Nature* **1999**, *398*, 788.

(9) Li, Y.; Somorjai, G. A. *J. Chem. Phys. C* **2007**, *111*, 9631.

(10) Jenniskens, P.; Blake, D. F. *Science* **1994**, *265*, 753.

(11) Usharani, S.; Srividhya, J.; Gopinathan, M. S.; Pradeep, T. *Phys. Rev. Lett.* **2004**, *93*, 048304.

(12) Zondlo, M. A.; Onasch, T. B.; Warshawsky, M. S.; Tolbert, M. A.; Mallick, G.; Arentz, P.; Robinson, M. S. *J. Phys. Chem. B* **1997**, *101*, 10887.

(13) Iedema, M. J.; Dresser, M. J.; Doering, D. L.; Rowland, J. B.; Hess, W. P.; Tsekouras, A. A.; Cowin, J. P. *J. Phys. Chem. B* **1998**, *102*, 9203.

(14) Pitzer, K. S.; Polissar, J. *J. Phys. Chem.* **1956**, *60*, 1140.

(15) Pursell, C. J.; Zaidi, M.; Thompson, A.; Gaston, C. F.; Vela, E. *J. Phys. Chem. A* **2000**, *104*, 552.

(16) Bournel, F.; Mangeney, C.; Tronc, M.; Laffon, C.; Parent, P. *Phys. Rev. B* **2002**, *65*, 201404.

(17) Gunster, J.; Liu, G.; Stultz, J.; Krischok, S.; Goodman, D. W. *J. Phys. Chem. B* **2000**, *104*, 5738.

(18) Smith, R. S.; Huang, C.; Kay, B. D. *J. Phys. Chem. B* **1997**, *101*, 6123.

(19) Souda, R. *Phys. Rev. Lett.* **2004**, *93*, 235502.

(20) Kang, H.; Shin, T.-H.; Park, S.-C.; Kim, I. K.; Han, S.-J. *J. Am. Chem. Soc.* **2000**, *122*, 9842.

(21) (a) Kang, H. *Acc. Chem. Res.* **2005**, *38*, 893. (b) Lee, C.-H.; Lee, P.-R.; Kang, H. *Angew. Chem., Int. Ed.* **2006**, *45*, 5529.

(22) Cooks, R. G.; Ast, T.; Pradeep, T.; Wysocki, V. H. *Acc. Chem. Res.* **1994**, *27*, 316.

(23) Schaff, J. E.; Roberts, J. T. *J. Phys. Chem.* **1996**, *100*, 14151.

(24) Sadtchenko, V.; Giese, C. F.; Gentry, W. R. *J. Phys. Chem. B* **2000**, *104*, 9421.

(25) Cyriac, J.; Pradeep, T. *J. Phys. Chem. C* **2007**, *111*, 8557.

(26) Cyriac, J.; Pradeep, T. *J. Phys. Chem. C* **2008**, *112*, 1604.

(27) Winger, B.; Laue, H.-J.; Horning, S.; Julian, R.; Lammert, S.; Riederer, D., Jr.; Cooks, R. G. *Rev. Sci. Instrum.* **1992**, *63*, 5613.

(28) Stähler, J.; Mehlhorn, M.; Bovensiepen, U.; Meyer, M.; Kusmierek, D. O.; Morgenstern, K.; Wolf, M. *Phys. Rev. Lett.* **2007**, *98*, 206105.

(29) Kimmel, G. A.; Petrik, N. G.; Dohnálek, Z.; Kay, B. D. *J. Chem. Phys.* **2007**, *126*, 114702.

(30) Su, X.; Lianos, L.; Shen, Y. R.; Somorjai, G. A. *Phys. Rev. Lett.* **1998**, *80*, 1533.

(31) Dohnalek, Z.; Ciolli, R. L.; Kimmel, G. A.; Stevenson, K. P.; Smith, R. S.; Kay, B. D. *J. Chem. Phys.* **1999**, *110*, 5489.

(32) Souda, R. *Phys. Rev. Lett.* **2004**, *93*, 235502.

(33) Parent, Ph.; Laffon, C.; Mangeney, C.; Bournel, F.; Tronc, M. *J. Chem. Phys.* **2002**, *117*, 10842.

(34) Cortenraad, R.; Denier van der Gon, A. W.; Brongersma, H. H.; Ermolov, S. N.; Glebovsky, V. G. *Phys. Rev. B* **2002**, *65*, 195414.

(35) Tzvetkov, G.; Ramsey, M. G.; Netzer, F. P. *J. Chem. Phys.* **2005**, *122*, 114712.

(36) Bay, H. L.; Winters, H. F.; Coufal, H. J.; Eckstein, W. *Appl. Phys. A: Mater. Sci. Process.* **1992**, *15*, 274.